npj | flexible electronics

Article

Published in partnership with Nanjing Tech University

https://doi.org/10.1038/s41528-026-00538-4

Scalable in-situ fabrication of multimodal electronic skin for intelligent robotics and interactive systems

Hakhyun Lim[1,3], Jungrak Choi[2,3], Chankyu Han[1,3], Dabin Kim[1], Hanbit Jin[2], Minki Kim[1], Yunjeong Kim[2], Jinhyeok Yang[1], Saerom Seo[2], Jaehoon Jung[1], Hunpyo Ju[2], Chan-Hwa Hong[2], Dongyoung Lee[2], Junseong Ahn[1] ✉ & Hye Jin Kim[2] ✉

Tactile sensing is a foundational technology for developing intelligent interactive systems across robotics, wearable devices, and human-machine interfaces. Despite progress in highly sensitive and multifunctional soft sensors, conventional multimodal platforms suffer from limited scalability and customization due to dependencies on complex cleanroom processes and labor-intensive assembly. Therefore, this study proposes a multimodal e-skin platform fabricated through a scalable, in-situ, and cleanroom-free strategy that integrates microporous-dielectric capacitive tactile sensors with UV-laser-patterned flexible circuitry in a single low-profile system. The approach facilitates rapid, application-specific layout design, enabling modular co-location of deformable pressure and bending sensors alongside compact IC modules for thermal and non-contact proximity sensing. In a representative robotic-gripper demonstration, microporous-dielectric pressure and bending sensors are integrated in a task-specific layout to match local contact geometry and functional demands. Additional validation across diverse applications, including robotic grippers, interactive toys, and pressure-mapping arrays, highlights the platform's adaptability and its system-level capacity to integrate seamlessly with tailored multimodal e-skin prototyping for complex real-world tasks.

Tactile sensing is essential for intelligent interaction in robotic systems[1–3], wearable electronics[4,5], and human-machine interfaces[6–10]. It allows machines or wearers to perceive pressure, deformation, and environmental stimuli, facilitating safe, adaptive behavior in dynamic or human-centered environments, such as haptic or interactive systems[11–14]. Soft tactile sensors have gained prominence for their mechanical compliance, conformability, and biocompatibility[15,16]. However, most have historically targeted single-modality detection, limiting their efficacy in complex tasks that demand multimodal perception[17,18]. Consequently, emerging applications, including object manipulation, physiological monitoring, and interactive control, therefore demand flexible and adaptive architectures that support spatially distributed, multimodal tactile sensing[19–21].

Recent advances in soft sensing have developed multimodal devices, particularly designed to mimic skin, that integrate pressure, strain, and temperature within a single platform[22,23]. To enhance sensing performance, these systems often utilize micro-structured elastomers, conductive composites, or hybrid materials[24–28]. However, most efforts have emphasized improving the performance of individual sensing components, such as sensitivity or multifunctionality. Consequently, these devices typically require complex lithographic fabrication or multilayer assembly, constraining scalability, conformability, and rapid prototyping, which are critical bottlenecks in current multimodal sensor platforms[29–31]. Furthermore, many platforms rely on manual, non-standardized assembly of discrete sensor components, leading to bulky structures, dense wiring, and alignment inconsistencies[32,33]. While printing and embedding techniques offer potential improvements[9], achieving scalable, application-specific integration of multiple sensing modalities with circuit-level functionality and high design flexibility remains a significant challenge.

This study proposes a multimodal e-skin fabricated using scalable, in-situ fabrication methods for intelligent robotics and interactive systems. The platform mimics human skin, which perceives various stimuli through specialized nerve receptors, such as Meissner's corpuscles for light touch, Pacinian corpuscles for vibration and deep pressure, Ruffini

[1]Department of Control and Instrumentation Engineering, Korea University, Sejong, Republic of Korea. [2]Electronics and Telecommunications Research Institute (ETRI), Daejeon, Republic of Korea. [3]These authors contributed equally: Hakhyun Lim, Jungrak Choi, Chankyu Han. ✉e-mail: junseong@korea.ac.kr; nolawara@etri.re.kr

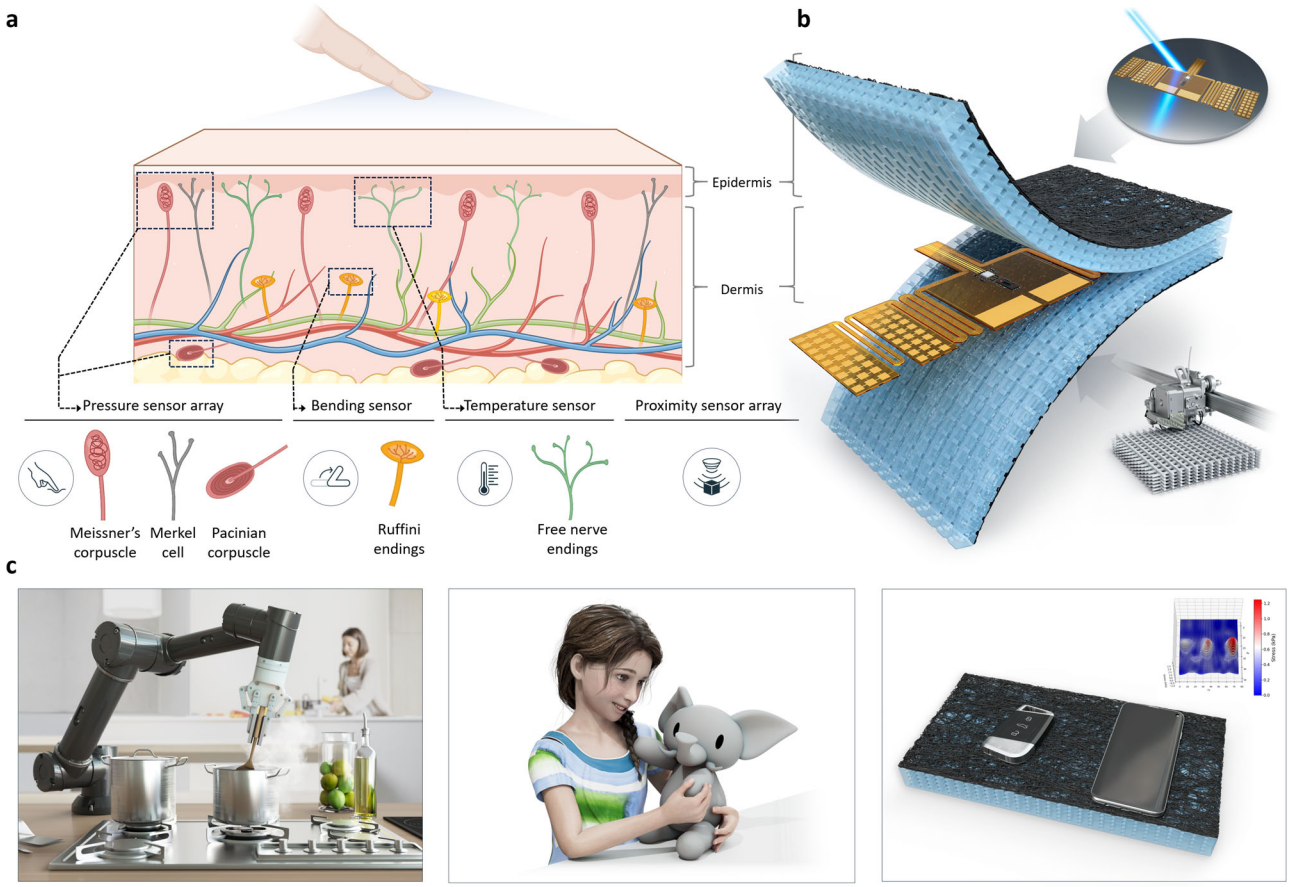

Fig. 1 | Concept and fabrication of the multimodal e-skin platform. a Human sensory receptors, including Meissner's corpuscles (light touch), Pacinian corpuscles (deep pressure), Ruffini endings (skin stretch), thermoreceptors (temperature), and replicated by corresponding sensor modules (created with Biorender). **b** Schematic of the in-situ fabrication integrating flexible circuits, porous dielectric layers, and IC-based modules into a unified platform. **c** Conceptual application scenarios of e-skin in robotic grippers, interactive toys, and pressure sensor arrays, highlighting its human skin-inspired multimodal sensing capabilities.

endings for skin stretch, and thermoreceptors for temperature. Furthermore, it incorporates visual perception of human eyes to provide depth and distance cues (Fig. 1a)[34–36]. This study develops an in-situ multi-sensor integration strategy that combines tactile sensing with a non-contact proximity channel, enabling more comprehensive and nuanced environmental interaction.

The multimodal sensor platform is fabricated using a unified prototyping strategy that integrates sensing and circuit elements into a single, low-profile system (Fig. 1b). Flexible circuits, patterned using ultraviolet (UV) laser techniques, support signal routing and modular sensor placement. Pressure and bending are measured through capacitive sensors made from a porous elastomeric dielectric layer and an electromagnetic interference (EMI)-shielding layer. Additional sensing modalities, such as temperature and proximity, are integrated using integrated circuit (IC)-based modules onto the flexible circuits. This fabrication approach enables customizable, single-platform integration of diverse sensors without complex or time-consuming post-processing. The platform's versatility is validated across multiple interactive use cases, including robotic grippers, interactive toy applications, and pressure sensor arrays, delivering robust multimodal feedback (Fig. 1c). The multimodal e-skin, customized for each application scenario, integrates tactile and visual-like sensing to mimic human-like perception of target objects. Overall, this work introduces a scalable, in-situ fabrication framework that translates material-level advancements in soft sensors into real-world deployment for next-generation interactive technologies.

Results

Overview of scalable in-situ fabrication of multimodal e-skin

Figure 2 outlines the concept and detailed workflow of scalable, in-situ fabrication of the multimodal e-skin platform. The strategy integrates flexible electronics with soft sensing elements into a mechanically robust yet compliant architecture. This unified, rapid prototyping involves three key stages: design and laser-based patterning of the flexible circuit, synthesis of a porous dielectric layer with an integrated CNT-based shielding layer, and final assembly into a unified tactile interface.

The fabrication begins with the preparation of the flexible circuit, acting as the electrical backbone of the sensor platform. Circuit paths, capacitive electrode arrays, and IC module layouts are custom-designed for specific applications. A glass wafer is purified with isopropyl alcohol (IPA) to eliminate surface contaminants and promote uniform surface wetting, creating capillary action, facilitating the conformal, temporary adhesion of a copper-coated polyimide (Cu/PI) film for subsequent processing (Fig. 2a(i)). A UV laser directly patterns circuit traces, electrodes, and mechanical features onto the Cu/PI films, enabling maskless, flexible circuit customization (Fig. 2a(ii) and Supplementary Fig. S1). This step verifies the feasibility of simple direct-write, maskless circuit fabrication for flexible electronics. Commercial IC modules (e.g., temperature and proximity sensors) are directly soldered onto the patterned copper pads using a low-temperature solder. This approach ensures robust electrical contact while protecting sensitive components from thermal stress. System-level integration is further achieved by attaching flexible flat cable (FFC) connectors to the circuit via anisotropic conductive film (ACF), establishing a reliable

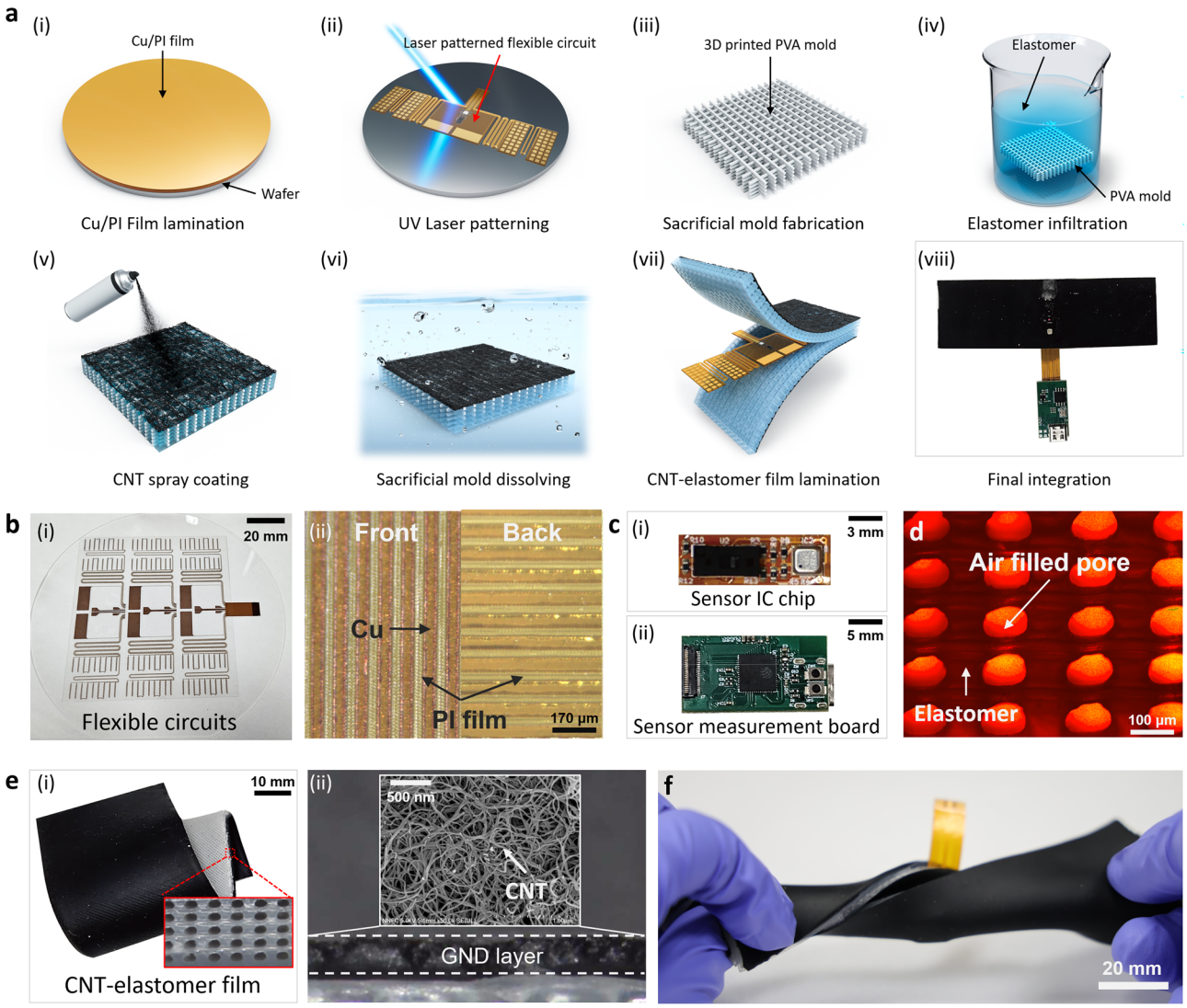

Fig. 2 | Fabrication process for the flexible circuit and carbon nanotube (CNT)-coated porous elastomer layer. a (i) Cu/PI film laminated onto an IPA-cleaned wafer. (ii) Direct-wire UV laser patterning of the flexible circuit. (iii) Fabrication of a sacrificial microporous PVA scaffold via 3D printing. (iv) Elastomer infiltration into PVA scaffold under vacuum, creating an elastomer-PVA composite mold. (v) CNT spray coating on the porous elastomer surface. (vi) Dissolution of PVA mold in water at 200 rpm to yield a microporous elastomer structure. (vii) Lamination of the porous CNT-elastomer film onto a patterned flexible circuit, embedding the circuit between elastomer layers. (viii) Final integration of the miniaturized multimodal sensing board with the porous elastomer layer. **b** UV-laser-patterned flexible circuit (i) overall view on glass wafer, and (ii) front and back views of the Cu/PI film. **c** (i) IC chip mounted on the flexible circuit. (ii) Sensor measurement board connected via an FFC connector. **d** Cross-section of porous elastomer film after PVA removal. **e** (i) CNT-coated porous elastomer layer for EMI shielding. (ii) SEM image of CNT ground network. **f** Structural and shielding stability under twisting.

interface with sensor measurement boards or external data acquisition circuits. This separation of on-board sensing functionality from external communication allows modular integration across various applications.

Subsequently, a microporous elastomeric dielectric layer is fabricated using sacrificial molding. A water-soluble polyvinyl alcohol (PVA) scaffold featuring a hexagonal pore array is additive manufactured, resulting in enhanced pressure sensitivity, mechanical compliance, and reduced hysteresis (Fig. 2a(iii))[18,37]. The PVA scaffold is immersed in a silicone elastomer, and a vacuum is applied to ensure thorough infiltration (Fig. 2a(vi)). A conductive layer for EMI shielding and electrical grounding is created by spray-coating the elastomer with a dispersion of multi-walled carbon nanotubes (MWCNTs) via mixing CNT powder with IPA, followed by sonication for uniform dispersion. This film provides effective EMI suppression and functions as a reliable ground (Fig. 2a(v)). This sacrificial PVA scaffold film is dissolved by immersing it in boiling deionized (DI) water, followed by rinsing to remove residues (Fig. 2a(vi)). The resulting porous elastomer film exhibits excellent elasticity (Supplementary Fig. S2) and consistent EMI shielding, rendering it suitable for high-sensitivity pressure and bending sensing (Supplementary Fig. S3).

During final assembly, the porous CNT-elastomer film is laminated onto the patterned flexible circuit through uncured elastomer-based bonding or mechanical interlocking methods, selected based on application requirements (Fig. 2a(vii)). The completed soft, conformable, and low-profile sensor platform supports multimodal measurements of pressure, bending, temperature, and proximity (Fig. 2a(viii)). Capacitive sensing enables high sensitivity and low hysteresis for pressure and bending measurements. Integrating diverse IC modules further expands sensing capabilities, as demonstrated by proximity sensing arrays (8×8 surface data) and temperature sensors. At the circuit layer, UV-laser patterning enables wafer-level fabrication of large-area Cu/PI flexible circuits, yielding a 60 μm minimum trace width with high edge definition. A sensor measurement board manages data acquisition and system control for modular integration (Fig. 2b, c). At the functional layer, a cross-section analysis post-PVA removal reveals a porous, air-filled elastomer that enhances sensitivity by

lowering stiffness and providing a compressible volume. A CNT-coated porous layer delivers EMI shielding with a continuous ground network, as confirmed by scanning electron microscopy (SEM) (Fig. 2d, e). The assembled film maintains structural integrity and shielding under torsional stress, underscoring mechanical robustness for practical applications (Fig. 2f). This fabrication technique enables the scalable and rapid prototyping of sensor platform designs tailored to diverse applications, including robotic grippers, interactive toys, and pressure-sensing arrays, while ensuring robust multimodal performance and durability.

Mechanism and sensor characterization of pressure and bending sensing

The pressure and bending sensors function on a self-capacitance principle, defined as the capacitance between an electrode and the electrical ground. This approach simplifies the sensor design, as each pressure or bending sensor can be conveniently integrated onto the flexible circuit as a single, dimensionally customizable electrode. Subsequently, the entire sensor platform is encapsulated by a soft porous elastomer layer and an outermost CNT coating on both sides, serving as the shared ground reference electrode. The capacitance of a parallel-plate capacitor is expressed as:

$$C = \frac{k\varepsilon_0 A}{d}$$

where C denotes capacitance, k represents the dielectric constant, ε_0 signifies the permittivity of free space, A refers to the surface area of the plate, and d is the distance between plates.

Applied external pressure from a universal testing machine (UTM) deforms the porous and CNT layers, reducing the separation between the sensing electrode and the grounded CNT layer and increasing the sensor's self-capacitance (Fig. 3a). Additionally, as the elastomer's dielectric constant is higher than that of air, the compression of the air-filled pores further increases the effective dielectric constant, enhancing the sensor's sensitivity.

Figure 3b illustrates the sensor's capacitance response to applied pressure, revealing a two-phase sensitivity profile: a high sensitivity (0.948 kPa^{-1}) under low pressures (<10 kPa) and a lower sensitivity (0.010 kPa^{-1}) under high pressures (>40 kPa). This behavior aligns well with established models for porous pressure sensors[38,39]. The capacitance changes due to a reduction in the electrode separation distance and an increase in the dielectric constant of the composite medium. At low pressures, the porous structure's low structural stiffness permits the electrodes to move closer as air pores compress. Simultaneously, as air within the pores is replaced by elastomer with a higher dielectric constant, the overall dielectric constant of the layer increases. At high pressures, once the pores are fully collapsed, the structure stiffens, minimizing further changes in electrode spacing and dielectric constant, reducing sensitivity. The sensor's high sensitivity at low pressures enables the sensor to detect minute increments as small as 10 Pa (Fig. 3c). Additionally, the sensor exhibits robust dynamic responses, independent of pressure application rate (Fig. 3d and Supplementary Fig. S4), with a rapid response time averaging ~0.60 s for rise and ~0.62 s for fall across various applied pressures. At 1 kPa, the rise and fall times are 0.65 s. At 10 kPa, the rise and fall times are 0.60 s and 0.37 s, respectively. At 100 kPa, the rise time decreases to 0.54 s, and the fall time increases to 0.58 s, highlighting the dynamic response across different pressure levels (Fig. 3e). The porous structure ensures low hysteresis of 3.66% (Supplementary Fig. S5) and consistent sensor performance over 10,000 loading-unloading cycles (Fig. 3f).

The bending sensor's response as a function of bending angle is depicted in Fig. 3g. The bending angle is defined as 0° when the sensor is flat and unbent. Bending causes the elastomeric layers to fold, reducing the distance between the electrode and the CNT ground layer. This mechanism is analogous to the low-pressure behavior of the pressure sensor, increasing capacitance. The bending sensor demonstrates rapid and stable responses up to 120° (Fig. 3h and Supplementary Fig. S6). Notably, the sensor exhibits lower sensitivity (~0.0012 per degree) at small bending angles (<20°) and higher sensitivity (~0.0061 per degree) at larger angles (>60°), displaying a nearly linear response in the higher angle region (60–120°). Under ideal uniform bending, the electrode near the neutral axis experiences minimal pressure and distance changes relative to the CNT ground layer, producing only small capacitance variations[40]. However, in practical applications (such as robotic grippers or wearable skin), bending is typically localized rather than uniform, inducing folding-like deformations[41]. Consequently, at small angles, capacitance changes remain limited, resembling the ideal scenario, but as bending angles increase, localized folding significantly reduces the electrode-ground layer distance, sharply increasing capacitance. Despite localized folding, the soft porous structure ensures high elasticity, yielding extremely low hysteresis of 1.44% for bending (Fig. 3h). Similar to the pressure sensor, the bending sensor demonstrates excellent dynamic response (Fig. 3i and Supplementary Fig. S7) and maintains consistent performance over 10,000 cycles (Fig. 3j). Additionally, integration of IC-based temperature and proximity modules within our platform enables accurate measurements of both modalities (Fig. 3k, l). Combining pressure, bending, temperature, and proximity sensors substantially broadens the sensing modalities, allowing customized sensor configurations for diverse application fields.

Application of e-skin for the robotic gripper and the interactive toy

Robotic grippers are increasingly employed in household and industrial robotics, assisting users in everyday tasks such as cooking, assembling, and handling delicate objects. Achieving human-like dexterity and sensitivity in such grippers necessitates sensors capable of perceiving tactile cues, including pressure, temperature, and deformation, comparable to those perceived by human senses. In household robots, where delicate interactions are common, soft tactile sensors are highly advantageous. To demonstrate the synergistic integration of our developed multimodal e-skin with robotic grippers, a representative cooking-assistance scenario was devised (Fig. 4a and Supplementary Movie S1). The e-skin, integrating pressure, bending, proximity, and temperature sensors, was mounted on the robotic gripper, enabling task execution based on comprehensive sensory feedback (Fig. 4b, c). For precise gripper control, the bending sensor is calibrated to map gripper-finger flexion sensing to corresponding signals, establishing a baseline (Fig. 4d). During the subsequent cooking-assistance task of retrieving a piece of bread from an oven, the robot initially uses proximity sensing to detect the object's local geometry and compensate for potential misalignment (Fig. 4e). Specifically, the proximity sensor provides an 8×8 multizone distance map over a square field of view (FOV) of approximately 60° × 60°. At representative pre-grasp distances (60–100 mm), this FOV corresponds to a sensing footprint of 65–120 mm per side, yielding an effective spatial sampling density of ~10 mm per pixel. This resolution is intentionally designed for coarse geometry perception to identify the object's relative position and orientation prior to contact. The gripper approach is algorithmically guided by monitoring the depth distribution across the 8 × 8 array; spatial depth gradients indicating misalignment are iteratively minimized to center the gripper. In practice, this allows the system to identify and correct misalignments of ~10–15 mm before physical contact is established (Supplementary Fig. S8). Next, the robot applies an optimal gripping force, determined from pressure and bending feedback, to prevent crushing or dropping the bread (Fig. 4g and Supplementary Fig. S9). Finally, the robot checks the bread's temperature, analogous to human thermal sensing, ensuring safe handover without burn risk (Fig. 4h). Although our demonstration focuses on retrieving and cooling a hot object before transferring it to a user, the synergy of multiple sensing modalities can significantly enhance robotic grippers across diverse applications (Supplementary Fig. S10).

Another practical application of the multimodal e-skin is in interactive toys, a growing field that fosters emotional engagement through sensory interaction, particularly for children. Tactile sensing significantly enriches user experience by enabling responsive, emotionally expressive interactions, supporting children's natural tactile exploration. To illustrate this potential,

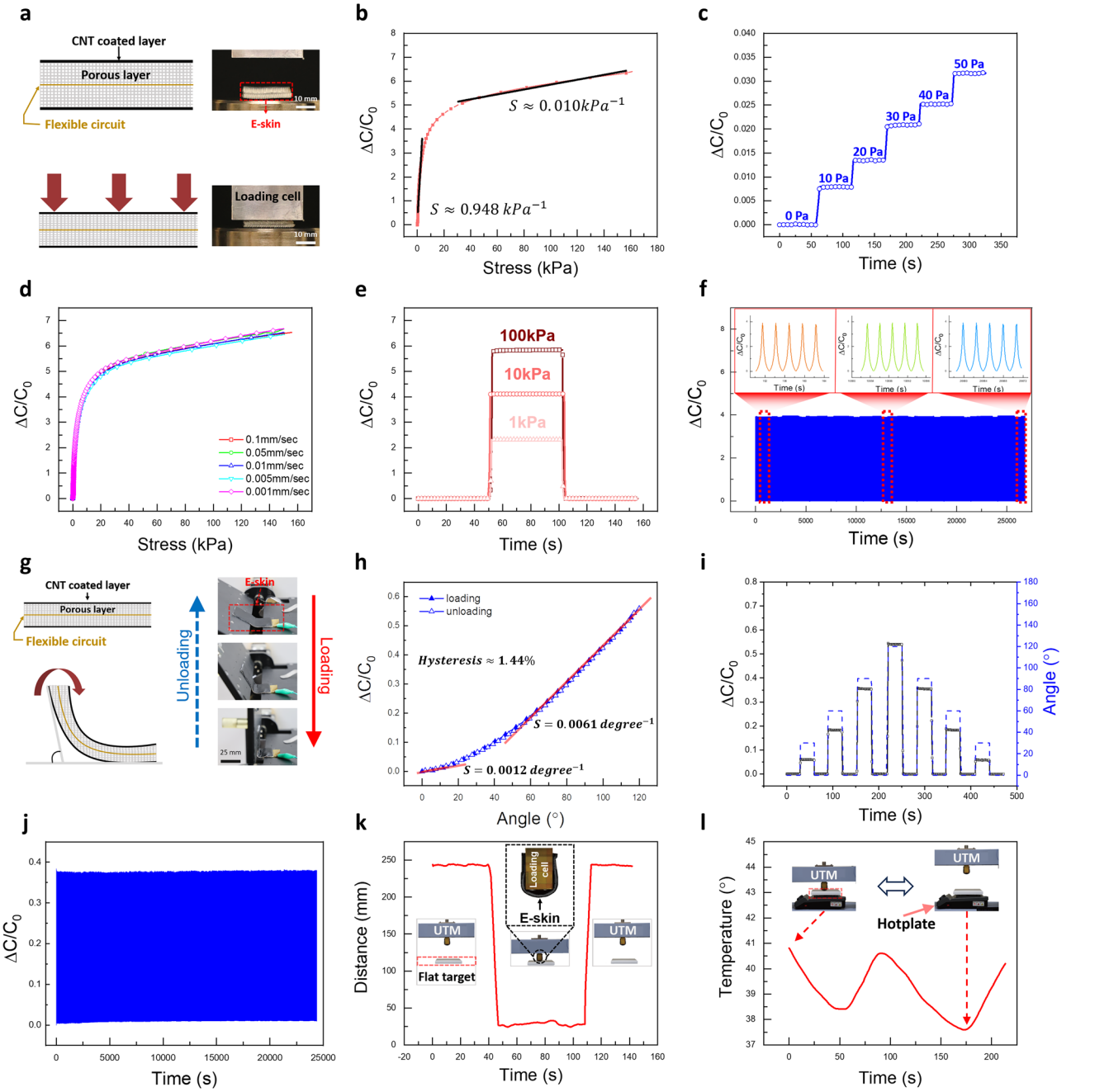

Fig. 3 | Pressure and bending sensor performance characterization. a Schematic of the pressure-sensing setup and mechanism. **b** Capacitance response under varying pressures (0–150 kPa). **c** Sensor response to incremental pressures (0–50 Pa) in the low-pressure regime. **d** Dynamic responses at different pressure loading rates. **e** Rise and fall times at 1, 10, and 100 kPa pressures. **f** Long-term stability under 10,000-cycle pressure loading. **g** Schematic of bending sensor deformation. **h** Capacitance responses across bending angles (0°–120°). **i** Dynamic capacitance under repeated bending. **j** Stability over 10,000 bending cycles. **k** Proximity sensor output at different distances. **l** Temperature sensor response at varying distances from the hotplate.

an interactive elephant toy was developed using elastomeric materials, additive manufacturing, commercially available electronic components, and the multimodal e-skin (Fig. 5a). The toy integrates various tactile sensing modalities, including pressure, bending, and temperature sensors, alongside actuators such as vibration motors, speakers, and LEDs (Fig. 5b, c).

A pressure sensor mounted onto the toy's chest simulates a realistic heartbeat by controlling a vibration motor, with vibration frequency and intensity modulated with applied pressure: higher pressure produces faster heartbeat-like vibrations, enhancing realism (Fig. 5d). A bending sensor embedded in the elephant's ear detects deformations when bending the ear, triggering an auditory response (e.g., "Hi! I'm elephant") via the integrated speaker when a bending threshold is exceeded (Fig. 5e). This system reliably registers events even under rapid, repetitive bending actions, ensuring robust and consistent responses during interactive play. Furthermore, a temperature sensor placed on the elephant's head detects warmth from skin contact, activating cheek-mounted LEDs when the threshold is reached to provide visual feedback (Fig. 5f). This demonstration underscores the versatility of the developed multimodal sensor platform, enabling rapid prototyping of interactive toys that seamlessly incorporate tactile, auditory, and visual feedback to enhance emotional engagement and play experiences (Supplementary Movie S2).

Overall, the developed e-skin fabrication method efficiently supports the design of multimodal tactile sensors, including proximity, pressure, bending, and temperature detection, while also integrating standard

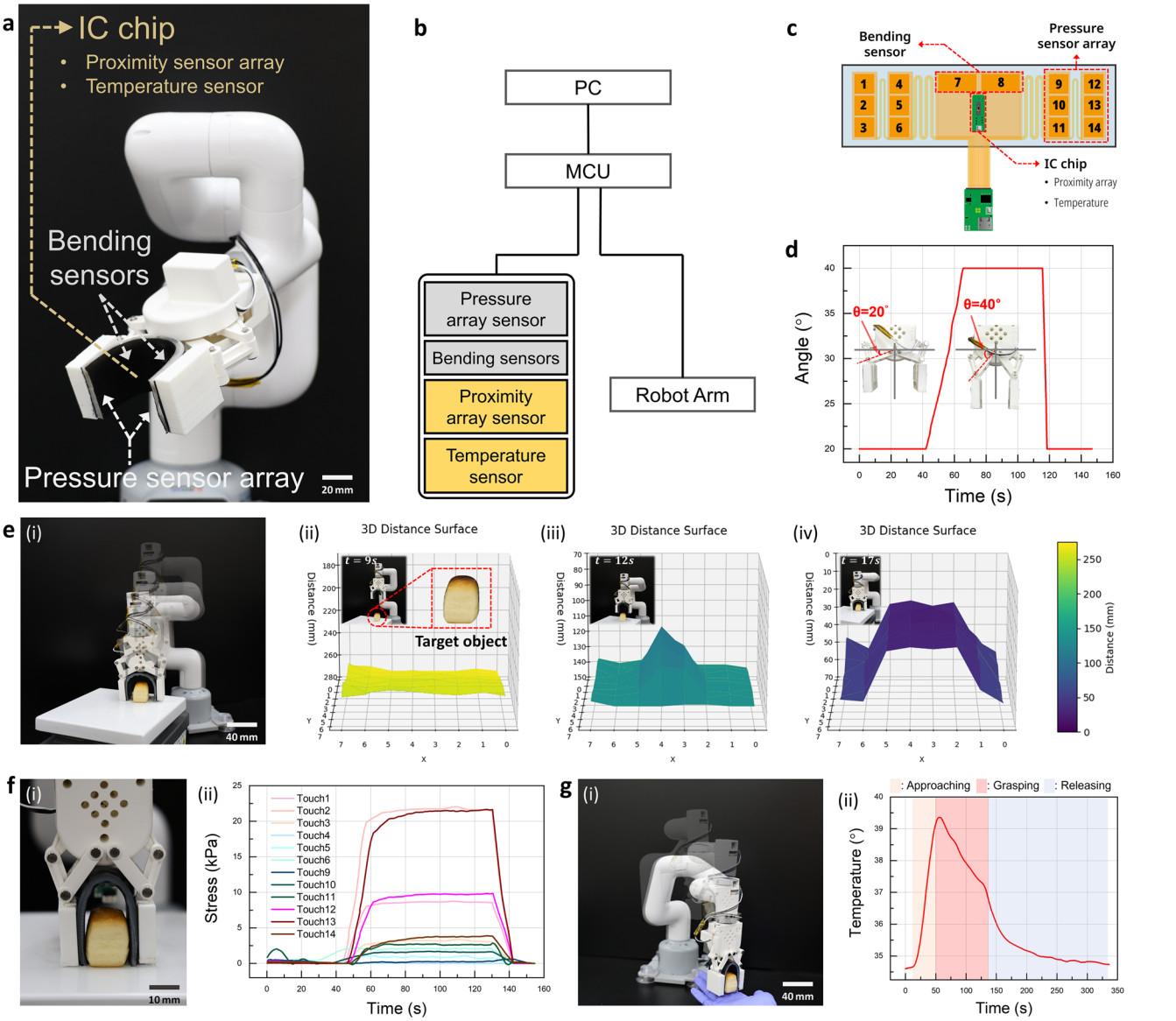

Fig. 4 | Application of the proposed e-skin-integrated robotic gripper in a cooking-assistance scenario. a Overview and **b** workflow of the developed gripper. **c** Sensor layout illustrating pressure sensor array indices, bending sensor location, and integrated IC chip. **d** Average change in bending-sensor capacitance during gripper deformation. **e** Proximity sensing: (i) sensor placement and approach direction; distance mapping results at (ii) $t \approx 9$ s (far distance): the 8 × 8 3D distance surface appears nearly flat; (iii) $t \approx 12$ s (intermediate distance): as the gripper moves closer, a shallow elevation reveals the target outline; (iv) $t \approx 17$ (near distance): at close range, the surface exhibits a pronounced peak and a clearer object contour, enabling precise localization. **f** (i) Gripping demonstration and (ii) corresponding pressure distribution measured by the pressure sensor array. **g** (i) Object handling and (ii) handover from the robotic gripper to the user once the temperature reaches a safe handling threshold.

electronic components, including actuators, LEDs, and speakers. The platform's rapid prototyping allows designers to readily tailor sensor layouts, geometries, and modality selection for different robotic grippers and task demands. The soft multimodal sensor platform streamlines prototyping and evaluation, markedly reducing design complexity and turnaround time.

Application to the pressure sensor array

The proposed e-skin fabrication method can produce multimodal sensing platforms and also support the simple fabrication of single-modality sensor arrays. Pressure sensors fabricated with this method exhibit a uniform porous structure, achieving high sensitivity and low hysteresis. The outermost CNT-based EMI-shielding layer provides compatibility with various conductive and non-conductive objects (Supplementary Fig. S11). Such pressure sensor arrays are critical in applications requiring spatially distributed force measurements, such as object recognition, posture monitoring, and robotic grasp analysis. These sensors detect both pressure magnitude and spatial distribution across surfaces, enabling nuanced interpretation of contact events (Supplementary Movie S3). The fabrication method facilitates rapid, accurate pressure mapping by pairing electrode arrays with microporous pressure-sensing films, as demonstrated with an 8 × 15 sensor array (Fig. 6a and Supplementary Fig. S12). A system-level demonstration employs this array in a smart weighing platform that measures the weights of multiple objects placed arbitrarily and computes their combined center of mass. Using gloved fingertip presses of varying directions and forces, the smart weighing system accurately identifies centers of mass for diverse object shapes and arrangements, and enables line-tracing tasks (Fig. 6b). Similarly, multi-touch operation is demonstrated by simultaneously applying conductive weights of different masses on the array, producing distinct pressure levels proportional to their masses (Fig.

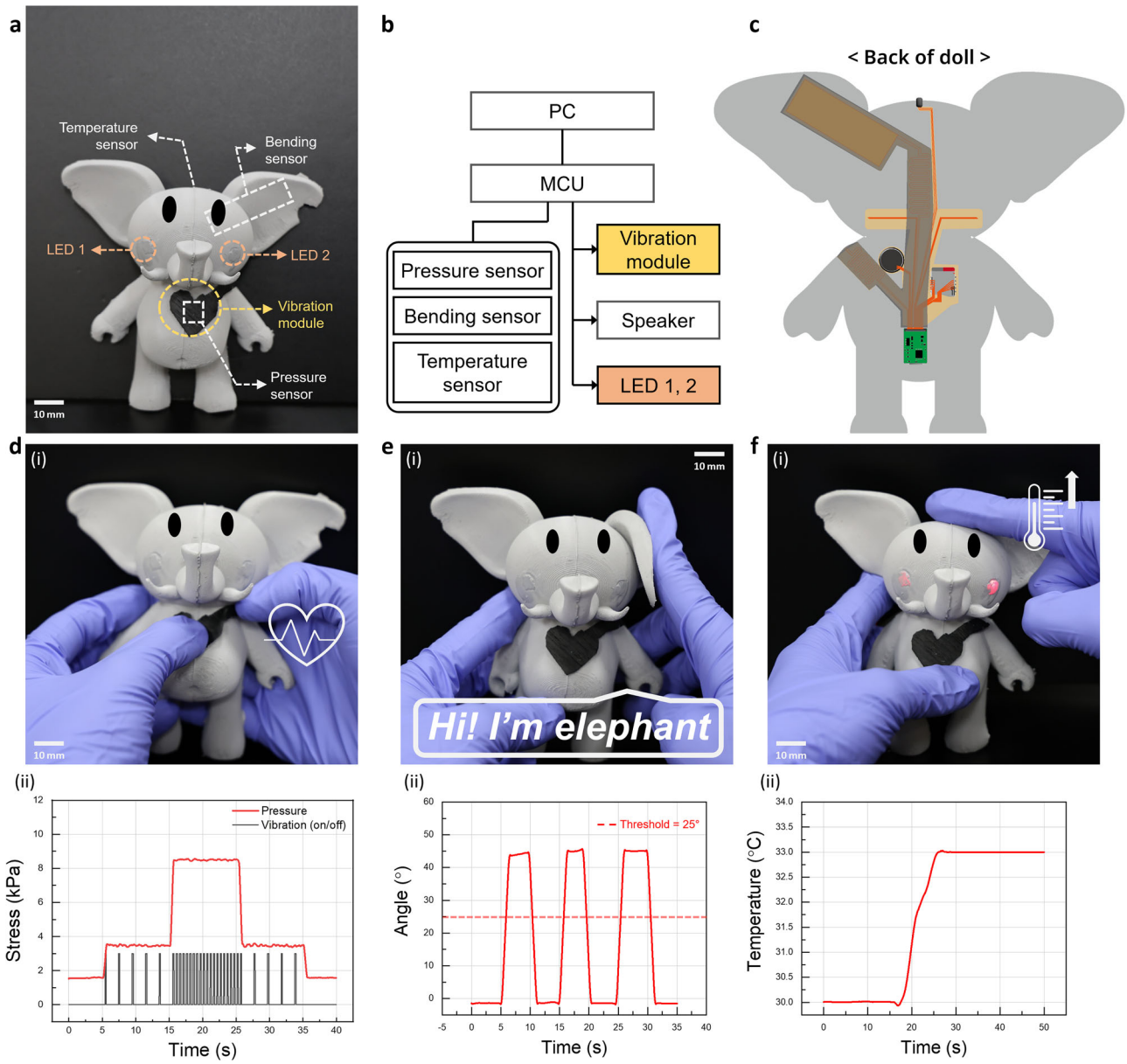

Fig. 5 | Application of the e-skin integrated interactive toy. a Overview, and **b** workflow of the toy. **c** Schematic of the positions of the integrated sensors and electronic modules. **d** Pressure interaction: (i) pressing the chest sensor, and (ii) corresponding pressure signal and vibration frequency response. **e** Bending-induced response: (i) folding the toy's ears, (ii) triggering audio playback, and capacitance response due to repeated ear bending. **f** Temperature sensing: (i) head sensor detects human body heat, and (ii) cheek LEDs illuminate when the preset temperature threshold is exceeded and turn off below the threshold.

6c). Position invariance is verified by placing identical weights at multiple locations, yielding consistent pressure distributions and validating stable, reliable sensor output (Fig. 6d). This functionality can be further extended to smart office and home systems for object identification or functioning as an interactive smart touch interface. Additionally, when 3D-printed letter stamps (e.g., "E," "T," "R," and "I") are pressed onto the sensor array, the resulting sensor readings distinctly reflect these shapes, highlighting the platform's high spatial resolution (Fig. 6e). The array's layout, resolution, and mechanical flexibility can be tailored for diverse applications. Furthermore, the platform's rapid prototyping capability enables swift adjustments to layout and material properties, accelerating design iterations and optimizing form factors and sensing performance.

Discussion

This study proposes a multimodal e-skin sensor capable of measuring pressure, bending, proximity, and temperature, developed through a scalable, integrated fabrication process that emulates key sensory functions of human skin. The sensors demonstrated high sensitivity, low hysteresis, rapid response, and long-term reliability under repeated mechanical deformation and pressure application. These characteristics closely mirror the adaptability and responsiveness of human skin to various stimuli. When integrated with flexible circuit substrates, the sensors prove effective across practical applications, including robotic gripping, interactive toys, and pressure mapping systems, showcasing their potential to enable intelligent, responsive systems capable of nuanced environmental interaction.

Despite these significant advancements, several limitations remain that warrant future research. First, although the proposed fabrication method is scalable and in-situ, it still involves manual alignment and lamination of separately produced flexible circuits and porous elastomer layers. This constraint may cause misalignment, reduced reproducibility, and hinder high-volume manufacturing. Future research could explore fully automated alignment, monolithic integration of all sensor layers directly onto the

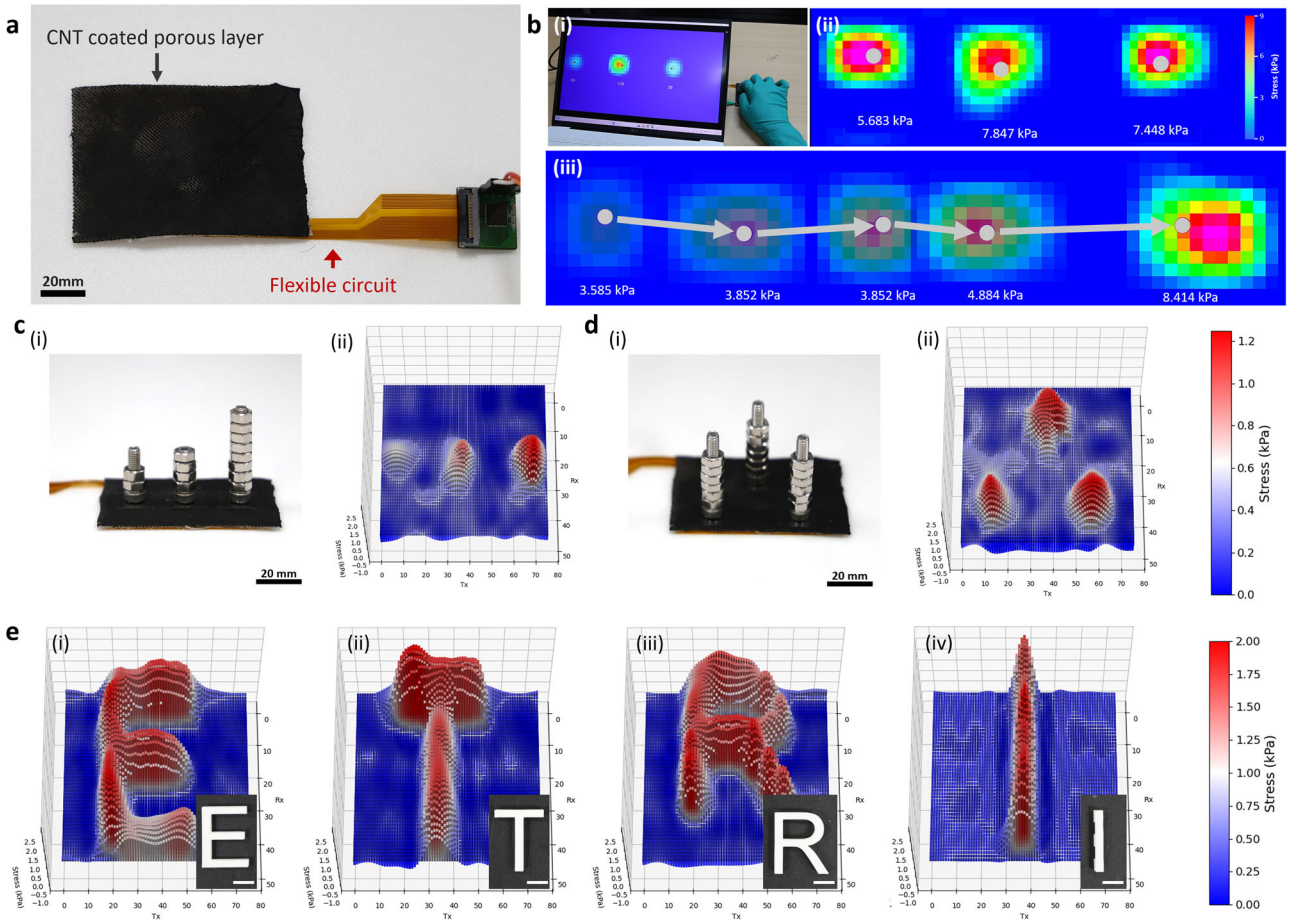

Fig. 6 | Application of the e-skin integrated pressure sensor array. a Overview of pressure sensor array structure integrated with flexible circuit. **b** Smart weighing system: (i) Overall setup: (ii) center-of-mass detection adapting to object shapes and arrangements using non-conductive objects; (iii) line tracing along a predefined path based on pressure-centroid tracking. **c** Multi-touch demonstration: simultaneous placement of weights produces distinct pressure levels corresponding to mass differences. **d** Position invariance: identical weights applied at different positions yield consistent pressure distribution across the sensor array, confirming stable and reliable sensor output. **e** Pressure mapping of letter-shaped stamps (E, T, R, I) pressed onto the sensor array, demonstrating high spatial resolution. Scale bar: 10 mm.

flexible substrate, or self-alignment approaches using alignment marks or mechanical interlocking structures.

Second, the current e-skin exhibits lower sensitivity at higher pressures (>40 kPa), potentially limiting its versatility and its applicability. Sensor performance across pressure ranges could be enhanced by tuning the conductive nanomaterial (e.g., CNTs) content in the elastomer according to percolation-threshold theory, adjusting the dielectric constant of the porous layer via high-k fillers (e.g., TiO_2) proportion dispersed in the elastomer, or controlling the porosity of the elastomer to modify mechanical response. Such tailored approaches could significantly broaden the applicability of the e-skin platform by enabling the fabrication of sensors with customizable sensitivities across diverse pressure ranges and allowing integration of multiple sensitivity levels within a single e-skin platform, better replicating the complex tactile characteristics of human skin.

Additionally, the sensor's two-phase sensitivity profile, with a noticeable reduction above ~40 kPa, could restrict its effectiveness in applications demanding high signal linearity and consistent responses over the entire pressure range. Implementing machine-learning-based calibration could mitigate this non-linearity, enhancing the e-skin's reliability and versatility in practical, real-world scenarios.

Therefore, this study constitutes a significant advancement in multimodal tactile sensing by introducing a straightforward, effective fabrication approach combined with robust performance (Supplementary Table 1). The developed e-skin holds considerable potential for intelligent robotics, interactive human-machine interfaces, and biomedical monitoring devices. Furthermore, the methodologies and performance benchmarks established in this research provide a valuable foundation for future developments in flexible and stretchable electronic sensor platforms.

Methods

Design and scalable in-situ fabrication of multimodal e-skin

The multimodal e-skin is fabricated through a detailed procedure encompassing flexible circuit preparation, microporous dielectric formation with CNT shielding, and final assembly. The flexible circuit acts as the sensor's electrical backbone. A glass wafer is cleaned using IPA to remove surface contaminants and promote uniform surface wetting, enabling temporary adhesion of the Cu/PI film via capillary forces. Circuit paths, sensor electrode layouts, and via-holes are defined using a UV laser system (MD-U100C, Keyence, Japan) operating in surface-etching or full-depth cutting modes, facilitating precise electrical routing and mechanical contouring. Commercial temperature (BME680, Bosch Sensortec, Germany) and proximity (VL53L5CX, Sparkfun Electronics, USA) sensing IC modules are soldered onto patterned copper pads using low-temperature solder. FFC connectors are subsequently bonded using anisotropic ACF to interface the flexible circuit with an external measurement board (ESP32-S3, Espressif Systems Co., China) or other data acquisition systems for multi-channel capacitive readout for system-level demonstrations. The microporous dielectric layer is fabricated through sacrificial molding. A PVA scaffold with a hexagonal pore array

(diameter ~180 μm, spacing ~150 μm, height ~2 mm) is produced with additive manufacturing using fused-deposition modeling 3D printing (Cubicon Style, Cubicon, Republic of Korea). A dispersion of MWCNTs (Carbon Nano-material Technology Co., Ltd., Korea) is then prepared by sonicating CNT powder with IPA at a 100:1 weight ratio with 0.5 wt% surfactant for 1 h to achieve uniform dispersion. This dispersion is spray-coated onto a 160 °C wafer using a 0.4 mm nozzle airbrush at 2 bar pressure, ensuring uniform coverage. The PVA scaffold is placed onto the CNT-coated wafer, and a silicone-based elastomer (Ecoflex 00-30, Smooth-on, USA; 1:1 base-to-curing-agent ratio) is poured onto the scaffold, vacuum-infiltrated for 20 min, hot-pressed using a flat press (QM900M, Qmesys, Republic of Korea), and cured at 60 °C for 1 h. The cured composite is peeled off and immersed in boiling DI water at 200 rpm for 12 h to dissolve the PVA template, followed by another 12-h rinse in clean DI water. The resulting porous CNT-elastomeric film is dried at 70 °C for 1 h. To integrate the components, an uncured elastomer is spin-coated at 500 rpm for 1 min (SF-100A, Rhabdos) onto the laser-patterned flexible circuit, forming a uniform interfacial layer. A single-sided CNT-coated porous elastomer is aligned and laminated on top. This structure is cured at room temperature for 2 h; the laminate is then carefully peeled off. The encapsulation is completed by repeating the lamination of the uncured elastomer to the opposite side of the laminate and spin-coating at 500 rpm for 1 min. After which, a second single-sided CNT-coated porous elastomer layer is aligned and laminated using the same method, followed by curing at room temperature for 2 h. This two-sided lamination embeds the flexible circuit within porous elastomer layers on both sides.

Mechanical characterization of multimodal e-skin

The mechanical stability of the sensors was evaluated through pressure and bending tests. For pressure testing, a multimodal e-skin sample (20 mm × 20 mm), comprising a laser-patterned flexible circuit encapsulated between two CNT-coated porous elastomer layers, was centered in a cylindrical holder. A UTM (AGS-X, Shimadzu, Japan), incremental loading-unloading cycles up to 150 kPa using a load cell (24.5 mm × 24.5 mm) larger than the sample area to ensure uniform pressure distribution. Capacitance responses of the sensor were simultaneously recorded using an LCR meter (E4980A, Keysight Technologies, USA). For the bending test, the multimodal e-skin sensor was mounted onto double-sided tape (56212, 3M, USA) fixed on a custom-built programmable bending machine. The sensor was bent incrementally from 0° to 120°, while capacitance responses were monitored using an LCR meter.

Electrical characterization of multimodal e-skin

The integrated IC sensors of the multimodal e-skin were electrically characterized through proximity and temperature sensing tests. For proximity sensing, the e-skin was attached to the UTM's load cell and aligned parallel to a flat plate surface. The load cell was translated vertically from the holder to precisely vary the distance between the sensor and the plate surface while recording sensor outputs. For temperature sensing, a similar configuration was used, with the sensor parallel and directed toward a 150 °C hotplate instead of the cylindrical holder. The sensor's tip was vertically moved from the hotplate, and its temperature readings were recorded.

Demonstration of multimodal e-skin for various applications

A robotic gripper experiment demonstrated the e-skin's integration with robotic systems for precise object handling through multimodal tactile feedback. A six-degrees-of-freedom robot (Mycobot 280, Elephant Robotics, China) was selected for its precision in delicate tasks in a controlled environment. A gripper (Mycobot parallel gripper, Elephant Robotics, China) was attached to the robot's end effector. To accommodate the gripper's narrow, short end, an auxiliary polylactic acid filament (DY PLA-ST, DYAIR, Republic of Korea) fixture was designed (Autodesk Fusion, Autodesk, USA) and 3D printed and affixed to the gripper's end. This fixture ensured stable, uniform pressure distribution on the sensor during object manipulation. The e-skin was attached to the gripper's end using double-sided tape. For real-time data acquisition, the e-skin was connected to an ESP32-S3 embedded board, using its native capacitive inputs (GPIO1–GPIO14) to read 12 pressure and two bending sensors. The embedded system was USB-powered (3.3 V) for benchtop experiments and supports battery-powered wireless operation, with a typical average current of <100 mA. Sensor data was collected and visualized in real time using Python. The experimental protocol was approved by the ETRI Institutional Review Board (IRB no. 2025-HR-0012).

An interactive toy was developed to enhance emotional engagement through tactile feedback, promoting natural exploration and interaction. The toy's bottom and top molds were designed using 3D modeling software, and a release agent (Easy-release 200, Mann Release Technologies, USA) was applied to its interior surfaces to facilitate separation of the elastomer. Elastomer, mixed with white dye (Silc Pig PMS white, Smooth-On, USA) and black dye (Silc Pig PMS black, Smooth-On, USA) at a 20:1 ratio, was poured into the molds and cured for one hour. The flexible circuit was mounted onto the bottom mold, and the top mold was aligned for encapsulation. Real-time pressure, bending, and temperature data were displayed in a Python interface. This experiment was approved by the ETRI Institutional Review Board (IRB no. 2025-HR-0012).

The pressure sensor array experiment evaluated the spatial pressure-mapping capabilities of the developed e-skin platform, enabling detailed interpretation of distributed contact events. A commercial projected-capacitance controller (IQS550, Azoteq (Pty) Ltd., South Africa) was interfaced with the flexible circuit, offering high sensitivity and low hysteresis suitable for multimodal sensing. Data acquisition and visualization were processed in real time using Python, which applied cubic interpolation to quadruple resolution, yielding a smoother and more detailed visual output. The resulting pressure map was displayed with a custom colormap for intuitive analysis. This setup provides an accurate representation of pressure distribution for real-time monitoring of contact events, facilitating a deeper understanding of the sensor array's performance in practical applications. This experimental protocol was approved by the ETRI Institutional Review Board (IRB no. 2025-HR-0012).

Data availability

The datasets generated and/or analyzed during the current study are not publicly available due to all data needed to evaluate the conclusions being present in the paper and/or the Supplementary Materials but are available from the corresponding author on reasonable request.

Code availability

There is no custom code or mathematical algorithm used in this manuscript.

Received: 1 September 2025; Accepted: 22 January 2026;
Published online: 29 January 2026

References

1. Jeong, Y. et al. Biomimetic, programmable, and part-by-part maneuverable single-body shape-morphing film. *Adv. Intell. Syst.* **5**, 2200293 (2023).
2. Mao, Q., Liao, Z., Yuan, J. & Zhu, R. Multimodal tactile sensing fused with vision for dexterous robotic housekeeping. *Nat. Commun.* **15**, 6871 (2024).
3. Li, G., Liu, S., Wang, L. & Zhu, R. Skin-inspired quadruple tactile sensors integrated on a robot hand enable object recognition. *Sci. Robot*. **5**, https://www.science.org (2020).
4. Wang, X. et al. Recent progress in electronic skin. *Adv. Sci.* **2**, 1500169 (2015).
5. Fastier-Wooller, J. W. et al. Flexible iron-on sensor embedded in smart sock for gait event detection. *ACS Appl. Mater. Interfaces* **16**, 1638–1649 (2024).
6. Qin, J. et al. Flexible and stretchable capacitive sensors with different microstructures. *Adv. Mater.* **33**, 2008267 (2021).
7. Zhu, M. et al. Haptic-feedback smart glove as a creative human-machine interface (HMI) for virtual/augmented reality applications. *Sci. Adv*. **6**, https://www.science.org (2020).

8. Liu, M. et al. A star-nose-like tactile-olfactory bionic sensing array for robust object recognition in non-visual environments. *Nat. Commun.* **13**, 79 (2022).
9. Han, H. et al. Battery-free, wireless multi-modal sensor, and actuator array system for pressure injury prevention. *Small* **20**, e2405493 (2024).
10. Fastier-Wooller, J. W. et al. Multimodal fibrous static and dynamic tactile sensor. *ACS Appl. Mater. Interfaces* **14**, 27317–27327 (2022).
11. Choi, J. et al. Thermoforming 2D films into 3D electronics for high-performance, customizable tactile sensing. *Sci. Adv*. **11**, https://www.science.org (2025).
12. Jung, Y. et al. Highly sensitive soft pressure sensors for wearable applications based on composite films with curved 3D carbon nanotube structures. *Small* **20**, e2303981 (2024).
13. Kim, K. et al. All-soft multiaxial force sensor based on liquid metal for electronic skin. *Micro Nano Syst. Lett.* **9**, https://doi.org/10.1186/s40486-020-00126-9 (2021).
14. Wu, P. et al. Advances in magnetic-assisted triboelectric nanogenerators: structures, materials and self-sensing systems. *Int. J. Extreme Manuf*. **6**, https://doi.org/10.1088/2631-7990/ad5bc6 (2024).
15. Gul, O. et al. Bioinspired interfacial engineering for highly stretchable electronics. *Nat. Commun.* **16**, 1337 (2025).
16. Liu, X., Wei, Y. & Qiu, Y. Advanced flexible skin-like pressure and strain sensors for human health monitoring. *Micromachines* **12**, https://doi.org/10.3390/mi12060695 (2021).
17. Wu, L. et al. Beetle-inspired gradient slant structures for capacitive pressure sensor with a broad linear response range. *Adv. Funct. Mater.* **34**, 2312370 (2024).
18. Choi, J. et al. Synergetic effect of porous elastomer and percolation of carbon nanotube filler toward high performance capacitive pressure sensors. *ACS Appl. Mater. Interfaces* **12**, 1698–1706 (2020).
19. Ates, H. C. et al. End-to-end design of wearable sensors. *Nat. Rev. Mater*. **7**, 887–907 (2022).
20. Niu, S. et al. A wireless body area sensor network based on stretchable passive tags. *Nat. Electron* **2**, 361–368 (2019).
21. Li, H. et al. E-tattoos: toward functional but imperceptible interfacing with human skin. *Chem. Rev*. **124**, 3220–3283 (2024).
22. Zhao, P. et al. All-organic smart textile sensor for deep-learning-assisted multimodal sensing. *Adv. Funct. Mater*. **33**, 2301816 (2023).
23. Yang, Y. et al. All-organic transparent plant e-skin for noninvasive phenotyping. *Sci. Adv*. **10**, https://www.science.org (2024).
24. Niu, H. et al. Perception-to-cognition tactile sensing based on artificial-intelligence-motivated human full-skin bionic electronic skin. *Adv. Mater.* **34**, 2202622 (2022).
25. Zhang, J. et al. Porous nanocomposites with enhanced intrinsic piezoresistive sensitivity for bioinspired multimodal tactile sensors. *Microsyst. Nanoeng.* **10**, 19 (2024).
26. Jeong, C., Ko, H., Jeong, H. E. & Park, Y. Bin. Shear-pressure multimodal sensor based on flexible cylindrical pillar array and flat structured carbon nanocomposites with simple fabrication process. *Compos. Sci. Technol.* **184**, 107841 (2019).
27. Mo, F. et al. A highly stable and durable capacitive strain sensor based on dynamically super-tough hydro/organo-gels. *Adv. Funct. Mater.* **31**, 2010830 (2021).
28. Zhang, S. et al. On-skin ultrathin and stretchable multifunctional sensor for smart healthcare wearables. *npj Flexible Electronics* **6**, 11 (2022).
29. Huang, Y. et al. A skin-integrated multimodal haptic interface for immersive tactile feedback. *Nat. Electron* **6**, 1020–1031 (2023).
30. Mao, Q., Liao, Z., Liu, S., Yuan, J. & Zhu, R. An ultralight, tiny, flexible six-axis force/torque sensor enables dexterous fingertip manipulations. *Nat. Commun.* **16**, 5693 (2025).
31. Ge, J. et al. A bimodal soft electronic skin for tactile and touchless interaction in real time. *Nat Commun.* **10**, 4405 (2019).
32. Lee, D. & Bae, J. Soft multimodal sensors with decoupled multimodality and minimal wiring for wearable systems. *Adv. Funct. Mater.* **34**, 2409841 (2024).
33. Zhao, S. et al. 3D dielectric layer enabled highly sensitive capacitive pressure sensors for wearable electronics. *ACS Appl. Mater. Interfaces* **12**, 32023–32030 (2020).
34. Waseem, A. et al. Self-powered and flexible piezo-sensors based on conductivity-controlled GaN nanowire-arrays for mimicking rapid- and slow-adapting mechanoreceptors. *npj Flexible Electronics* **6**, 58 (2022).
35. Hong, S. J. et al. Bio-inspired artificial mechanoreceptors with built-in synaptic functions for intelligent tactile skin. *Nat. Mater.* https://doi.org/10.1038/s41563-025-02204-y (2025)
36. Tsuji, S. & Kohama, T. Proximity and tactile sensor combining multiple ToF sensors and a self-capacitance proximity and tactile sensor. *IEEJ Trans. Electr. Electron. Eng.* **18**, 797–805 (2023).
37. Cavallo, A. et al. A biocompatible pressure sensor based on a 3D-printed scaffold functionalized with PEDOT:PSS for biomedical applications. *Org Electron* **96**, 106204 (2021).
38. Wang, J. et al. A highly sensitive and flexible pressure sensor with electrodes and elastomeric interlayer containing silver nanowires. *Nanoscale* **7**, 2926–2932 (2015).
39. *2015 Transducers - 2015 18th International Conference on Solid-State Sensors, Actuators and Microsystems* (IEEE, 2015).
40. Yuxin, P. et al. Recent advances in flexible bending sensors and their applications. *Int. J. Smart Nano Mater.* **15**, 697–729 (2024).
41. Su, Y., Wu, B., Chen, W. & Destrade, M. Finite bending and pattern evolution of the associated instability for a dielectric elastomer slab. *Int J. Solids Struct.* **158**, 191–209 (2019).

Acknowledgements

This work was supported by the Korea Evaluation Institute of Industrial Technology (KEIT) grant funded by the Korea government (MOTIE, Grant No. RS-2022-00154781, Development of large-area wafer-level flexible/stretchable hybrid sensor platform technology for form-factor-free highly integrated convergence sensor), and by Electronics and Telecommunications Research Institute grant (26ZB1100), and supported by a Korea University Grant. The funders had no role in study design; data collection, analysis or interpretation; manuscript writing; or the decision to submit the work for publication.

Author contributions

H.L., J.C., C.H. contributed equally to this work. H.L., J.C., C.H., J.A., and H.J.K. conceived and designed the study. H.L., C.H., D.K., H.B.J., M.K., Y.K., and J.Y. performed materials preparation, device fabrication, and sensor characterization. S.S., J.J., H.P.J., C.-H.H., and D.L. developed the readout electronics and carried out system-level integration and validation. H.L., J.C., and C.H. curated data, conducted analyses, and prepared the figures. H.L., J.C., and C.H. wrote the initial draft. J.A. and H.J.K. supervised the project, provided resources and funding, and revised the manuscript. All authors discussed the results, contributed to the interpretation, and reviewed and approved the final manuscript.

Competing interests

The authors declare no competing interests.

Additional information

Supplementary information The online version contains supplementary material available at https://doi.org/10.1038/s41528-026-00538-4.

Correspondence and requests for materials should be addressed to Junseong Ahn or Hye Jin Kim.